The Hula Valley subsurface structure inferred from gravity data

Michael Rybakov,[a] Lorian Fleischer,[a] and Uri ten Brink[b]
[a]Geophysical Institute of Israel, P.O. Box 182, Lod 71100, Israel
[b]U.S. Geological Survey, 384 Woods Hole Road, Woods Hole, Massachusetts 02543, USA

ABSTRACT

Rybakov, M., Fleischer, L., ten Brink, U. 2003. The Hula Valley subsurface structure inferred from gravity data. Isr. J. Earth. Sci. 52: 113–122.

We use the 3-D gravity inversion technique to model the shape of the Hula basin, a pull-apart basin along the Dead Sea Transform. The interpretation was constrained using the Notera-3-well density logs and current geological knowledge. The model obtained by inversion shows a rhomb-shaped graben filled with approximately 4 km of young sediments in the deepest part of the basin. The reliability of this model was verified using 3-D forward modeling with an accuracy of 0.5 km. Curvature attributes of the gravity field depict the main fault pattern, suggesting that the Hula basin is a subsiding rhomb-shaped graben, bordered by steep-sided, deep basement faults on the western and eastern sides (Qiryat Shemona and Jordan River faults) and by gradual, en-echelon step faults on the southern and northern margins of the basin.

INTRODUCTION

The Hula basin is the northernmost Plio-Pleistocene extensional basin in Israel, located along the Dead Sea transform fault (Fig. 1, insert). The basin is situated between the Naftali Mountains in the west and the Golan Heights in the east. To the north, the Metulla High and Mount Hermon block the Hula Valley, while to the south the basin is closed by en-echelon faults of the Korazim Plateau (Heimann, 1990). The bedrock of the depression is probably composed of Eocene, Senonian, or Cenomanian rocks (mainly carbonates) that are exposed along the western boundary of the basin. Sedimentation in the basin probably began in the Middle–Late Miocene, represented by predominantly fluvio-lacustine fresh water deposits such as marl, lacustrine limestone, sand, gravel, peat, and lignite.

This sequence was repeated several times during Pliocene and Pleistocene times. Basalt flows and tuffs originating from the surrounding area interrupted the sedimentation in the basin and alternate with the fluvio-lacustine environment (see Heimann, 1990, for the flow direction).

The volcanics may be correlated with the surface sections based on absolute age determination. Their greater thickness in the subsurface within the basin indicates that the basin was depressed relative to the surrounding areas. The earliest volcanics penetrated by the Notera-3 well (TD-2781 m) are the "Lower Basalt" dated at 8.8 Ma. Later volcanic activity in the basin is represented by several basalt flows such as the "Cover Basalt" (3.1–4.1 Ma), "Mesky and Dalton
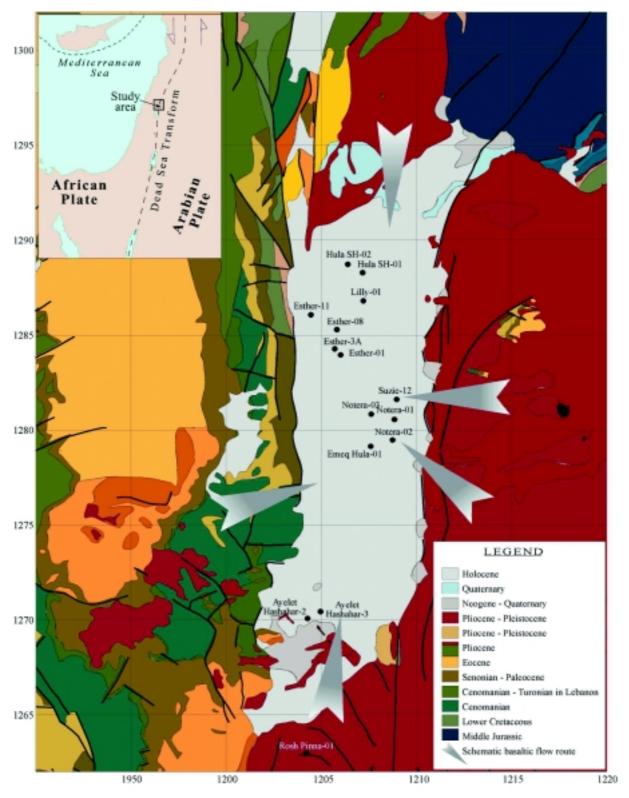
E-mail: rybakov@gii.co.il

Fig. 1. Geological map of the Hula Valley (after Sneh et al., 1998) superimposed by the well location and schematic basaltic flow routes (Heimann, 1990). Insert—tectonic setting of the study area.

Basalts" (2.72 Ma), and the "Dalwe and Hasbani Basalts" (1.13–1.36 Ma) (Heimann, 1990).

The upper 1200 m of the penetrated section in the Esther-1 well (TD-1293 m), Lilly-1 well (TD-1260 m), Notera-3 well, and other shallower wells, such as Notera-1 (TD-505 m), Notera-2 (TD-749 m), Suzie-12 (TD-479 m), etc., were deposited during the Pleistocene in a pluvial and interglacial regime. Extended rivers and lakes developed over the whole Hula basin. Peat, sand, and lumachelle interbeds are common in the upper part of this sedimentary sequence.

The graben occupying the Hula Valley is about 20 km in length and 6 km wide. The subsided block is bordered by steep basement faults between the western "Qiryat Shemona" master fault, which runs along the foot of the Naftali Mountains, and the eastern, main strike-slip "Jordan River" fault. Toward the north, the western master fault splits into two segments, the Roum and Yammunneh faults, and the eastern main fault turns northeast at Mount Hermon, diminishing in the Rachaya and Serjaya faults (Heimann, 1990).

The southern limit of the Hula graben toward the elevated Korazim block is represented by a few en-echelon faults trending WNW–ESE such as Kefar Hanasi, Rosh Pinna, and Yesud HaMa'ala faults (Kashai and Crocker, 1987; Heimann, 1990; Frieslander, 1997). The northern limit of the graben is represented by a series of gradual step faults, such as the Kefar Yuval, Ma'ayan Baruch, and Hagosherim faults trending NW–SE (Heimann, 1990, Gardosh et al., 2001).

The first extensive gravity survey in the area was carried out by the Institute for Petroleum Research and Geophysics (IPRG), now the Geophysical Institute of Israel (GII), in 1965–66 (Yuval, 1966). The gravity data were interpreted in 2-D mode by Yuval (1966), which gave a thickness of 1600 m for the young fill sediments, and by Folkman (1980), which calculated a maximum fill thickness of 2 km. These calculations were based on general geological considerations owing to the fact that no deep well had been drilled in the Hula basin at that time. A dense gravity survey was recently conducted in the northern area of the Golan Heights, Mount Hermon, and the northern Hula Valley (Rybakov et al., 1997; Rybakov and Goldshmidt, 2000; Rybakov et al., 2001).

In 1981 the Notera-3 well was drilled near the geographical center of the Hula Valley to a depth of 2781 m, penetrating a series of fluvio-lacustine sediments alternating with peat, lignite, and some basaltic flows of Pliocene–Pleistocene ages. Based on the density log from the Notera-3 well, a mean value of 2.3 g/cm^3 was selected by Klang (1984) for the basin fill and, with a 2-D gravity interpretation program, a maximum thickness of 4600 m was calculated for the Hula Valley.

In this paper the gravity data were inverted for the thickness of the basin fill by using a new 3-D iterative gravity inversion technique developed by Jachens and Moring (1990). A reliability check of the final solution was performed using the 3-D Gravity and Magnetic Modeling Program (IGMAS—Prof. Goetze, Dr. Schmidt, and Gravity Research Group, Institute for Geological Sciences, Free University of Berlin). We also used the Notera-3 density log to constrain the 3-D gravity interpretation by the actual densities.

This work was intended to produce a structural map of the bedrock of the Hula basin fill and to delineate the subsurface fault pattern. The results will assist in the study of the tectonics and basin configuration of this area.

GRAVITY DATA

The gravity data were taken from the GII Gravity Database. There are 2,200 stations in the study area (white dots on Fig. 3): 550 stations located on the basement rock surrounding the Hula Valley and approximately 1,650 on the basin fill. The station spacing in the Hula Valley itself is dense, on the order of 400–500 m. Outside the valley, the spacing ranges from 500 m to 2 km or more, with reasonably uniform coverage throughout the area. The raw gravity data were reduced using several standard procedures. The latitude correction was calculated according to the 1967 Geodetic Reference System Formula. The gravity data were reduced using 2.67-g/cm^3 density. Terrain correction was calculated using relief in the form of a digital terrain model with a 25-m grid, adopted from the Digital Terrain Model (DTM) compiled by J.K. Hall (Hall, 1993). These data sets were carefully checked for erroneous values and gridded using a kriging technique at 250-m spacing, slightly smoothed, and presented in the complete Bouguer gravity map (Fig. 3).

Figure 3 shows a prominent gravity low over the Hula Valley with a magnitude reaching 26 mGal. This low is about 6.5 km at its widest point, which is close to the width of the flat part of the valley. The anomaly is about 14 km long, which is less than the length of the flat part of the Hula Valley (22 km). Two high gradient zones (reaching 8 mGal/km) bound this negative

anomaly on the western and eastern sides, and these gravity steps correspond well to the Qiryat Shemona and Jordan River master faults. The gravity gradients on the northern and southern anomaly closures are smaller (about 4 mGal/km). This suggests that the fill thickness changes gradually in a N–S direction. No signature of the master faults extension to the north is seen in the gravity pattern.

DENSITY DATA

In order to estimate the depth to the base fill using gravity, we need to know (or at least be able to assume) the density contrast between the bedrock and the fill. Previous works that interpreted the gravity in the Hula Valley used a bedrock density value of 2.6 g/cm^3 and a constant density contrast of –0.5 g/cm^3 (Folkman, 1980) and –0.3 g/cm^3 (Klang, 1984). Using a number of density logs (Rybakov et al., 1999), we estimated a mean bedrock density value of 2.67 g/cm^3. This density is typical for the Mesozoic carbonate rocks surrounding the Hula Valley and outcropping in Mt. Hermon, the Galilee, and, partially, in the Golan Heights. The value is also consistent with the density chosen using the Nettleton (1971) approach. This method analyzed a correlation between the topography and the Bouguer gravity values calculated with various densities, and the most suitable density value was assumed to be 2.67 g/cm^3, which caused the least influence of relief features on the resulting gravity data.

The Notera-3 well, drilled in the center of a structural low (Kashai and Goldberg, 1984; Heimann, 1990) at the location of the minimum of the gravity anomaly (Fig. 3), provided important information on the geological background for accurate gravity interpretation. The Notera-3 density logs show a complicated pattern of density distribution (Fig. 2); however, an increasing density to depth is clearly identified. This trend corresponds partially to the sedimentary compaction with depth. We calculated the depth–density correlation for unconsolidated clastic sediments on a number of the density logs in the Eastern Mediterranean, the coastal plain, and the Dead Sea Transform valley (Rybakov et al., 1999, and dashed gray line in Fig. 2). Relatively high average densities are typical for the intervals with the intercalated basalt layers, with density values reaching up to 2.9 g/cm^3. For 3-D inversion and forward modeling the density model was assumed as follow:

1. Uppermost (0–500 m) layer, a value of 2.03 g/cm^3; the layer corresponds to the clastic sediments of the Notera Fm., the top and bottom of the deeper layers assumed arbitrary;
2. Second (500–1,500 m) layer, a value of 2.27 g/cm^3;
3. Third (1,500–2,500 m) layer, a value of 2.40 g/cm^3; and
4. Fourth, deepest (from 2,500 m) layer, a value of 2.47 g/cm^3.

The four-layer model provides a better approximation of the density log and is an improvement over the use of a single density value for the whole basin fill. It should also be noted that the mean density value of the whole interval (2.26 g/cm^3) is very close to Klang's estimation (2.3 g/cm^3). However, using the four-layer model will result in a smaller calculated total thickness of the basin fill, as will be demonstrated below.

METHODS

In this study, we used three computer programs, thus providing the most advanced technology of combined interpretation now available. A description of the program algorithms is provided in the Appendix.

The negative gravity anomaly was inverted for thickness of the Hula basin fill using the 3-D depth-to-basement method (DEPTH2BS). The scattered gravity data were gridded at 250 m spacing and were separated into two input files, one for the gridded gravity in the basin, and the other for the surrounding basement. The density within the basin fill was divided into four layers (Fig. 2). Although it is reasonable to suppose lateral density variations in the basin fill, none of those encountered had sufficient consistency to justify a more complicated density model.

To estimate the reliability of the solution obtained by the 3-D inverse method, we calculated the confidence intervals using the 3-D forward modeling (IGMAS system). Second derivatives were calculated to deduce the shallow fault pattern. Using the CURVATURE program we calculated the curvature attributes on the Bouguer gravity of the Hula Valley. The attributes were as follow: dip-curvature, mean-curvature, minimal-curvature, and maximal-curvature. The comparison of the various curvature attribute maps with known geological and tectonic features suggested that the curvature attributes reveal a significant amount of valuable information relating to faults, lineaments, and other tectonic features. Our experience showed that amongst a number of derivatives of gravity potential, the dip-curvature attribute is most easily understandable and provides the most information for studying shallow tectonics (Fig. 4).
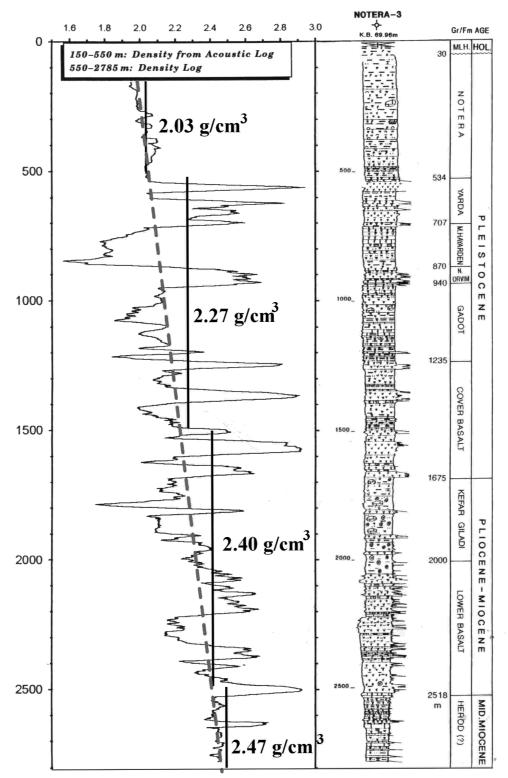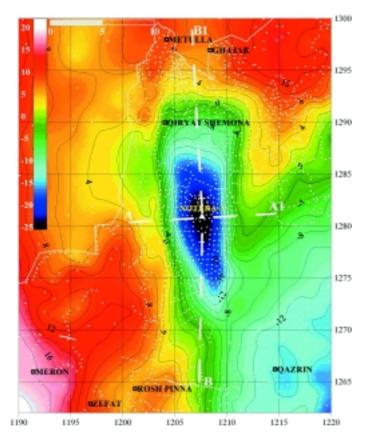
Fig. 2. Composite log of Notera-3 well (Rybakov et al., 1996). Dashed gray line shows the depth–density relationship for unconsolidated clastic sediments defined on a number of density logs in the Eastern Mediterranean, coastal plain, and the Dead Sea Transform valley. Thick black lines denote the interval mean density values used for 3-D inversion.
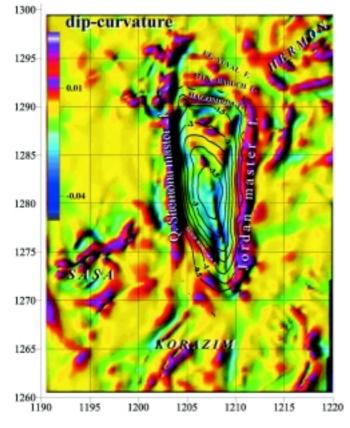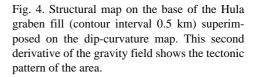
Fig. 3. Complete Bouguer gravity map of the Hula Valley and vicinity with the location of the Notera-3 well and the structural profiles. Contour interval is 2 mGal. White dots denote gravity stations.

Fig. 4. Structural map on the base of the Hula graben fill (contour interval 0.5 km) superimposed on the dip-curvature map. This second derivative of the gravity field shows the tectonic pattern of the area.
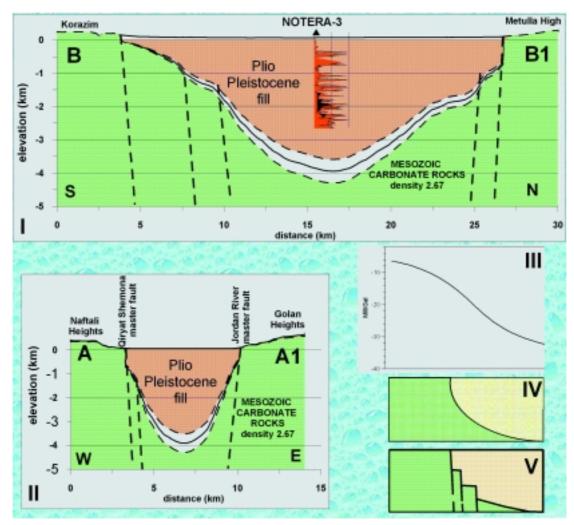
Fig. 5. Structural profiles A-A1 (II) and B-B1 (I) derived from the 3-D gravity interpretation (for location, see Fig. 3). Horizontal and vertical scales are the same. Solid graph denotes the best-fit model; the dashed lines bound the 91% confidence interval examined by 3-D forward modeling. III—gravity effects of the listric model (IV) and a series of small faults (V) are no different under prevailing conditions.
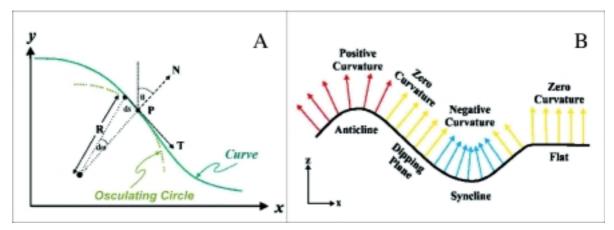

Fig. 6. Mathematical definition of curvature (A) and the sign convention for curvature attributes (B) (after Roberts, 2001, and Schmidt, pers. comm.). See Appendix for details.

RESULTS AND DISCUSSION

The iterative procedure DEPTH2BS separated the gravity field into a bedrock gravity component and a basin gravity component caused by variations in the thickness of the basin fill. The basin component has been inverted to the fill thickness using the density model. The basin model predicts a maximum thickness of 4 km at the location of 1207.5 N/1281.2 E (Israel grid).

Based on these results, a structural map on the base fill has been created (contour lines in Fig. 4). Figure 5 presents the west–east- and north–south-oriented structural profiles crossing the Hula Valley close to the Notera-3 well. The thickness of the fill varies dramatically over short distances in an E–W direction. Comparing these results with the geological map (Fig. 1), we suggest that the abrupt thickness changes of the basin fill represent the subsurface continuation of the Jordan River and Qiryat Shemona master faults (Fig. 4). Moreover, the curvature map suggests that the Hula basin is a rhomb-shaped graben. However, in the northern and southern directions, the basin closes less abruptly than in the E–W direction (Fig. 5). The dip-curvature pattern at the southern closure of the Hula basin appears to be an expression of the en-echelon fault system with a possible listric character. The resolving power of the gravity does not allow us to distinguish between the gravity effects of the listric fault or a series of small faults, and no direct evidence of the listric character was observed in the study area. However, the same dip-curvature pattern was calculated at the southern closure of the Dead Sea graben where the Amaziahu fault was imaged as listric (Kashai and Crocker, 1987). The northern margin seems to be more complicated than the southern: the linear north-to-south-oriented lineament in the central part of the basin corresponds to the deepest structural axis of the basin. West and east of the lineament, the uppermost sedimentary layers are slightly raised. A number of other lineaments can be delineated in the Korazim block, Sasa structure, and Mt. Hermon.

In general, the results obtained from the potential field data are inherently non-unique. The present interpretation should also be considered as one possible solution that could produce gravity patterns matching the observations. The estimated values of the density and calculated depths should be regarded as rough estimates; it is therefore important to estimate the reliability of the proposed model. The location is more reliably defined than the subsurface basin shape. The deeper parts of the model give rise to the longer wavelength, smaller amplitude anomalies and, hence, limit the resolution. The relatively simple density model (four layers) can be altered using a more complicated depth–density pattern (Fig. 2).

The geometry of the Hula basin obtained from the DEPTH2BS program and the four-layer density model were examined in order to estimate the final solution reliability using the IGMAS program (3-D forward modeling). The confidence intervals of the basin fill thickness were calculated using several models varying in fill and country rocks densities. The 91% confidence intervals are about 0.5 km. The difference between the calculated anomalies of the simple 4-layer and complicated depth–density models is negligible. Using forward modeling we analyzed the gravity effects of variously shaped basins. The results suggest that the gravity effect (Fig. 5III) of the basin with a round bottom (Fig. 5IV) is not significantly different from the gravity effect of the box-shape basin (Fig. 5V). This means that under prevailing conditions (gravity station spacing, accuracy of the survey, density contrasts, etc.) the resolving power of the gravity does not facilitate making a choice between these models.

CONCLUSION

The structural map on base fill in the Hula Valley has been prepared for the first time based on 3-dimensional routines. In addition, the lineaments in the dip-curvature map confirm the rhomb shape of the basin, revealing the pattern of the subsurface faulting.

ACKNOWLEDGMENTS

REFERENCES

Folkman, Y. 1980. Magnetic and gravity investigations of the Dead Sea rift and the adjacent areas in northern Israel. Journal of Geophysics 48: 34–39.

Frieslander, U. 1997. High resolution seismic survey in the Hula Valley and Park Ha Yarden areas. GII Rep. No. 647/162/96.

Gardosh, M., Bruner, I., Rybakov, M., Burg, A., Bein, A. 2001. Seismic study in the northeast Hula Valley. GII Report No. 452/90/01 and GSI Report No. 4/2001 (in Hebrew).

Goetze, H.-J., Lahmeyer, B. 1988. Application of three-dimensional interactive modeling in gravity and magnetics. Geophysics 53, 8: 1096–1108.

Hall, J.K. 1993. The GSI Digital Terrain Model (DTM) completed. GSI Current Research: 5: 47–50.

Heimann, A. 1990. The development of the Dead Sea rift and its margins in northern Israel during the Pliocene and the Pleistocene. Ph.D. thesis, Hebrew Univ., Jerusalem and GSI Rep. 28/90, 76 pp.

Jachens, R.C., Moring, B.C. 1990. Maps of the thickness of Cenozoic deposits and the isostatic residual gravity over basement for Nevada, U.S. Geological Survey Open-File Report, 90–404, 11 pp.

Kashai, E.L., Crocker, P.F. 1987. Structural geometry and evolution of the Dead Sea–Jordan rift system as deduced from new subsurface data. Tectonophysics 141: 33–60.

Kashai, E.L., Goldberg, Y. 1984. Notera-3, geological completion report. Oil Exploration in Israel Report 84/20, 76 pp.

Klang, A. 1984. A new interpretation of the gravimetric anomaly of the Hula basin, IPRG Report X1/776/81 (1), 3 pp.

Nettleton, L.L. 1971. Elementary gravity and magnetic for geologists and seismologists. SEG, Monograph Series, No. 1:121.

Roberts, A. 2001. Curvature attributes and their application to 3D interpreted horizons. First Break 19.2: 85–100.

Rybakov, M., Goldshmidt, V., Fleischer, L., Gvirtzman, G., Goldberg, I., Sorin, V. 1996. Interpretation of gravity and magnetic data from Israel and adjacent areas: investigation results. IPRG Report R04/313/95.

Rybakov, M., Goldshmidt, V., Fleischer, L., Goldberg, I., Weiner, D. 1997. Interpretation of gravity and magnetic data from Israel and adjacent areas. IPRG Report No. 840/19/96

Rybakov, M., Goldshmidt, V., Rotstein, Y., Fleischer, L., Goldberg, I. 1999. Petrophysical constraints on gravity/magnetic interpretation in Israel. The Leading Edge 18, 2: 269–272.

Rybakov, M., Goldshmidt, V., 2000. Gravity survey in the northern Hula area. GII Report No. 852/52/99.

Rybakov, M., Goldshmidt, V., Fleischer, L., Ben-Gai, Y. 2000. 3-D gravity and magnetic interpretation for the Haifa Bay area (Israel). Journal of Applied Geophysics 44, 4: 353–367.

Rybakov, M., Goldshmidt, V., Fleischer, L., Reznikov, M. 2001. Study of the subsurface geology in Israel and adjacent area using gravity, magnetic and seismic reflection data. GII Report No. 840/75/00.

Sneh, A., Bartov, Y., Weissbrod, T.E., Rosensaft, M. 1998. Geological map of Israel, 1:200,000. Geol. Surv. Isr.

Yuval, Z. 1966. Jordan Valley gravity survey. IPRG Report, No. GR/427/66.

APPENDIX

METHODOLOGY

The following three new programs complete the advanced computer technology for combined interpretation used in our previous works (Rybakov et al., 2000):

1. 3-D depth to basement method (DEPTH2BS)

This method (Jachens and Moring, 1990) requires knowledge of the residual gravity field, exposed geology, and vertical density variation within the Cenozoic basin deposits. Drill hole information and geophysical data that provide constraints on the thickness of the basin fill are also input to the model. The method separates the gravity field into two components, one caused by variations of density within the pre-Cenozoic bedrock and another caused by variations in thickness of the Cenozoic basin fill. To accomplish this process, the gravity data are separated into observations made inside the depression and on bedrock outcrops. The inversion is complicated by two factors: (1) bedrock gravity stations are influenced by the gravity anomaly caused by low-density deposits in nearby basins, and (2) the bedrock gravity field varies laterally because of density variations within the bedrock. The inversion presented here does not take into account lateral variations of the Cenozoic sediment density. To overcome these difficulties, a first approximation of the bedrock gravity field is determined by interpolating a smooth surface through all gravity values measured on bedrock outcrops. The basin gravity is then the difference between the observed gravity field on the original map and the first approximation of the bedrock gravity field, and is used to calculate the first approximation of the thickness of Cenozoic deposits. The thickness is forced to zero where bedrock is exposed. This first approximation of the bedrock

gravity is too low near the basin edges because of the effects of the nearby low-density deposits on the bedrock stations. The bedrock gravity station values are "corrected" for the effects of the low-density deposits (the effects are calculated directly from the first approximation of the thickness of the Cenozoic deposits), and interpolating a smooth surface through the corrected bedrock gravity observations makes a second approximation of the bedrock gravity field. This iteration leads to an improved estimate of the basin gravity field, an improved depth to bedrock, and a new correction to the bedrock gravity values. This procedure is repeated until successive iterations produce no significant changes in the bedrock gravity field.

2. 3-D forward modeling

The gravity data were interpreted using the IGMAS system developed by Prof. Goetze, Dr. Schmidt, and their gravity research group at the Free University of Berlin (Goetze and Lahmeyer, 1988). This three-dimensional interactive modeling allows integrated processing and interpretation of gravity and magnetic fields, yielding an improved geological model. Generally, our 3-D models of the earth's lithosphere are constructed by triangulated polyhedral with constant density and/or magnetic susceptibility. Interactive modifications of model parameters (geometry, rock density, and susceptibility) enable us to design the model as realistically as possible. Other constraining data sets from seismic reflection and/or refraction surveys access the numerical modeling process and direct visualization of both calculated and measured gravity and magnetic fields. We used 3-D forward modeling to estimate the confidence intervals of the solution obtained by the 3-D inverse approach.

3. Curvature attributes

The collection of filtration techniques of potential fields (polynomial regional-residual separation, derivatives computation, up-down continuation, Fourier transformations) for qualitative interpretation of gravity and magnetic data was recently completed by the curvature attributes calculation method. Curvature belongs to a group of second derivatives and is a three-dimensional property of the surface. For a particular point on a surface, its curvature is defined as the rate of change of direction of a surface (Fig. 6). This describes how bent a surface is at a particular point on the surface, i.e., how much the surface deviates from a plane at this point. Thus, the curvature controls the local area change when the surface is dilated. A sphere having the greatest possible contact with the surface is called the osculating sphere. The radius of this osculating sphere is defined as the radius of curvature, and curvature is the reciprocal of the radius of curvature.

The program calculating the curvature of a gridded surface was developed by Dr. S. Schmidt (Free University of Berlin). We used the program to calculate the curvature attributes on the Bouguer gravity of the Hula Valley. The attributes are as follows: dip-curvature, mean-curvature, minimal-curvature, maximal curvature, etc. Maps of the various curvature attributes were compared (calibrated) with known geological and tectonic features. The comparison suggested that the curvature attributes reveal considerable valuable information relating to faults, lineaments, and other tectonic features.

It should be emphasized that no interpretation technique should be used in isolation. All the results should be integrated with reference to the original geological information and this requires extensive image manipulation in order to extract the full benefit.